On the realization of microscopic grids for local strain measurement by direct interferometric photolithography

Raphaël Moulart[a], René Rotinat[a,*], Fabrice Pierron[a], Gilles Lerondel[b]

[a]*Laboratoire de Mécanique et Procédés de Fabrication (EA 4106), Ecole Nationale Supérieure d'Arts et Métiers, rue Saint-Dominique, B.P. 508, 51006 Châlons-en-Champagne CEDEX, France*

[b]*Laboratoire de Nanotechnologie et d'Instrumentation Optique, Université de Technologie de Troyes - CNRS (FRE 2671), 12 rue Marie Curie B.P. 2060, 10010 Troyes CEDEX, France*

Abstract

In order to extend the application range of the so-called "grid method" to the micron scale and thus quantitatively characterize the micromechanical behavior of metallic alloys, we report in this paper on the optimization of microscopic 2D gratings with pitches ranging from 1 to 10 μm. After an overview of the state of the art on full-field kinematic measurements at the micron scale, the direct interferometric photolithography technique, used to produce such gratings, is introduced. The shape of the gratings has been characterized using an atomic force microscope and compared with the theoretical profiles. An optimization of the parameters involved in the marking process is then presented. One of the goals lies in the measurement of displacement fields using spatial phase-shifting concept which is briefly recalled. This optimization is achieved for two different optical techniques used to observe the grids namely optical microscopy and white light confocal interferometry. Finally, a first evaluation of the performance of the measurement technique is given and discussed.

Keywords: Full-field measurement; Grid method; Microscale; White light interferometer

1. Introduction

The thorough knowledge of the mechanical behavior of materials requires a study of the physical phenomena at the scale of the heterogeneities. Actually, the global behavior of a material can be predicted from relevant microscopic data through the use of homogenization schemes. A number of powerful schemes are available nowadays. The major difficulty of this approach remains, however, the determination of the local properties as the characterization of the individual components of a material (single crystal for a metal, fibres and matrices for composites) is not enough to predict the global mechanical properties. Indeed, the interactions between the individual constituting elements are not taken into account (defaults and grain boundaries in a metallic alloy, interphase of a fibre reinforced polymer). In this context, the development of quantitative displacement and strain field measurements at this scale is an important field of great interest and still remains a scientific challenge.

As a part of the effort to understand better the local behavior of metallic alloys, this work aims at developing a microextensometric method designed to detect the initiation of microplasticity. Indeed, plastic stretching of polycrystalline metals involves a complex heterogeneous distribution of strain fields depending on the crystallographic orientations of the different grains. Locally, strain values can be very high, even when the nominal strain remains under the macroscopic yield point. This

*Corresponding author.

E-mail addresses: raphael.moulart@chalons.ensam.fr (R. Moulart), rene.rotinat@chalons.ensam.fr (R. Rotinat), fabrice.pierron@chalons.ensam.fr (F. Pierron), gilles.lerondel@utt.fr (G. Lerondel).

effect, called microplasticity, will drive the global response of the material especially under high cycle fatigue.

At this scale, point measurements (with gauges for instance) are no longer suitable. New techniques have to be developed. An interesting alternative is the use of full-field measurements. Based on optical concepts, these techniques allow to get a mapping of strain fields over a large region of interest. To study the onset of microplasticity, the required strain resolution should be around 10^{-4} with a spatial resolution in the order of 30 μm (typical grain size for the material considered here, i.e., a low carbon steel). To the best knowledge of the present authors, this target cannot be reached with the available methods, as confirmed by the following section.

2. State of the art

Several types of kinematic full-field measurement techniques exist, with a number of them suitable at the micron scale. At this scale, in addition to the usual criteria taken into account to select one method (nature of the pattern, algorithm of detection and processing), another important issue has to be considered. The way the field will be digitized (by white light observation, electronic microscopy or scanning probe microscopy to cite only the major options) is of a great importance as it can strongly influence the metrological performances.

In order to position our work with respect to the current state of the art, a survey of the existing techniques will be proposed with the following logical organization:

- nature of the pattern encoding the surface to study;
- measurand and corresponding algorithm or method used to extract it;
- procedure used to detect the signal.

2.1. Periodic pattern

The methods that use a periodic pattern to encode the surface allow to study the displacement fields (phase shifting methods) or directly the strain fields (manually exploited moiré method). The patterns used are often uni- or bidirectional (cross) gratings obtained by different techniques. These techniques will be shortly reviewed in Section 3. The main advantage of these techniques is their high resolution (directly depending on the pitch of the grating). Three different types of algorithm can be distinguished, as follows.

2.1.1. "Manually" exploited moiré

Moiré methods are based on the analysis of interferences between a regular grating of parallel lines and another grating of comparable pitch but deformed [1]. The first grating is used as a reference whereas the second one is attached to the surface of the sample. The resulting fringes represent isovalue lines of the displacement component perpendicular to the reference grating lines. The average normal strain in the direction perpendicular to the lines can be calculated over a region of interest as follows:

$$\varepsilon_x = \frac{N_x \times p}{l_x}, \tag{2.1}$$

where ε_x is the strain in the x direction, N_x the number of moiré fringes in the region of interest and l_x the length of the region of interest (in the x direction).

This "manual" exploitation provides a direct and simple determination of a mean value of ε over the region of interest. However, this procedure leads to a poor sensitivity as the manual fringe counting can be done only with a resolution of about ± 0.5 fringe.

With the development of robust phase extraction algorithms (see Section 2.1.2), this kind of fringe exploitation has been abandoned at the macroscopic scale. However, it is still used at the microscopic and nanoscopic scales. Sometimes, the reference grating can be a numerical one: there is no physical representation of it and the usual interference phenomenon is replaced by arithmetical or logical operations with a virtual reference grating generated by a computer [2]. The reference grid can also be the grid of a CCD sensor associated with an optical microscope with pitches going from a few micrometers to a few tens of micrometers [3].

To reach smaller pitches, other techniques have to be used. The "SEM-moiré" uses the scanning lines of a scanning electronic microscope (SEM) as the reference grid that allows to decrease the pitch down to 100 nm [4–7]. The scanning lines of a focused ion beam (FIB) can also be used [8]: the principle is the same as the SEM but electrons are replaced by gallium ions (Ga^+) which are heavier and thus more sensitive to atomic displacement.

For sub-nanometric pitches, scanning probe microscopy is required (AFM or STM) [9–11]. In some cases, the atomic lattice can even directly be used as the sample grating [9].

These techniques using SEM or scanning probe microscopy present a very high spatial resolution; nevertheless, the time needed to digitize the surface can be a limitation (with transitional phenomena for instance).

2.1.2. Phase extraction methods

In mechanics, when an interference phenomenon is occurring (with coherent light or white light), it can be easily demonstrated that the phase of the interference fringes is directly proportional to the displacement of the related geometric point. Thus, by determining the phase at each point, the whole in-plane displacement field of the considered surface can be known.

2.1.2.1. Semi-global detection by Fast Fourier Transform.

By applying a Fast Fourier Transform algorithm over a given region of interest, it is possible to calculate the mean value of its phase [12,13].

Zhao and Asundi used this technique associated with optical microscopy, a SEM and an atomic force microscope (AFM) [14]. The spacial resolution is p, the pitch of the grating (833 nm), the displacement resolution is between p/N and $0.5p$ (if N is the number of pixels sampling one period of the grid) .

2.1.2.2. Local detection by phase shifting methods. Phase shifting methods allow to get the phase of periodic fringes at every pixel and thus get the displacement field. By applying a known phase shift between several recordings, the phase can be calculated using linear combinations of the different recordings [15].

The periodic signal processed by the phase shifting algorithm can be moiré fringes [6,16,17]. This allows to have a displacement value for each pixel of the recorded image (obtained using scanning probe microscopy) and can thus be a more quantitative extension of the traditional moiré exposed in Section 2.1.1.

The fringes can also be obtained by moiré interferometry. This technique combines high displacement sensitivity and high spatial resolution [18,19]. A thin cross-lines phase diffraction grating is replicated onto the specimen surface to study. The interaction between two coherent laser beams with the deformed grating produces interference fringes representative of the induced displacement. Localization [20] and microscopic inspection of heterogeneous deformation in coarse-grained polycrystalline metals [21,22] can be visualized with this method.

Finally, the periodic processed signal can also be the grating itself [23] but until now, and to the best knowledge of the present authors, this technique has not been applied at this scale.

The main advantage of phase shifting methods associated with periodic phenomena (gratings or interference fringes) is their high displacement resolution (around a few percents of the pattern pitch).

2.2. Random pattern (speckle)

The methods that use a random pattern allow to study the displacement fields by temporal phase shifting methods (interferometry) or by digital image correlation (DIC method). Their main advantage is that preparation of the surface to study is not always necessary. The roughness of the surface can be used as the random pattern itself or generate it when illuminated by a coherent light. However, the nature of the signal induces a reduced signal to noise ratio and a lower spatial resolution for the DIC methods.

2.2.1. Speckle interferometry (using phase shifting)

When a rough surface is illuminated with a coherent light beam, the latter is reflected in all directions from the surface. The reflected beams will interfere with one another and generate a speckle pattern (multi-beam interferences). By building up interferences between the speckle patterns with the specimen at rest and loaded, regular fringes directly related to the displacement are observed. These fringes are then processed by a temporal phase shifting algorithm to extract the displacement information for every pixel [24,25].

A few applications of this technique exist at a microscopic scale, for instance to study the mechanism of cracking of thin films (with a displacement resolution of 0.3 μm) [26] or to study the deformation of a porous alumina membrane under pressure [27].

2.2.2. Digital image correlation (DIC)

DIC methods give access to displacement information by calculating the so-called cross-correlation function between the unloaded and the loaded states [28,29].

Usually, the encoding is obtained by applying a layer of white paint onto the surface and then spraying it with a black aerosol. At the micron scale, this simple procedure to get a random pattern cannot however be directly transposed. A possibility is to project a titanium powder in a polymeric phase at the surface of the sample [30]: this technique allows to get images through an optical microscope and a CCD camera with a sufficient contrast. The application of such a technique is limited by the resolution of the optical microscope. Another possibility to obtain a random pattern is to use the "speckle effect" introduced in the previous section [31]. At this scale, the surface roughness itself can also be considered as a random pattern by using scanning probe microscopy (AFM or STM) [32–37] or scanning electronic microscopy (SEM) [35,36]. The digitizing resolution of the profile can thus reach a few nanometers (for a field of view of a hundred of square micrometers for instance). One of the advantages of the DIC methods is the fact that they do not always require a difficult preparation of the surface. Moreover, they can be adapted to 3D problems [38] even with original applications such as medical ones [39]. Nevertheless, the main drawbacks of these techniques are the low displacement resolution as the measurements are noisy (due to the random nature of the pattern) [40] and also a low spatial resolution (depending on the size of the correlation windows).

2.3. Summary and conclusion

Table 1 summarizes the studies mentioned in this section and compiles the different references previously cited.

The aim of the present project is to characterize the local mechanical behavior of metallic grains at the micron scale. In order to achieve the required performances (strain resolution around 10^{-4} with a spatial resolution in the order of 30 μm), none of the above method were completely suitable. The previous experience of some of the authors with the grid method at the macroscopic and mesoscopic scales led to the idea of adapting it at the micron scale. However, in order to achieve this, two problems have to be addressed. First, a grid has to be "printed" onto the specimen. Direct interferometric photolithography was

Table 1
Summary of the existing techniques and corresponding references

Pattern	Periodic			Random	
Measurand	Strain	Phase of fringe pattern		Phase of fringe pattern (ESPI)	Displacement
Algorithm/analysis	Manually exploited moiré	FFT	Phase shifting	Phase shifting	DIC
Observation					
Optical	[3]	[14]	[20–22]	[26,27]	[30,31]
SEM	[4–7]	[14]	[16,17]	X	[35,36]
AFM/STM	[9–11]	[14]	[6,17]	X	[32–37]

thought to be both convenient and fast, compared to scanning or mask lithography (see Section 3). Then, the grids have to be digitized (i.e., "read") in order to determine the in-plane displacement field by the grid method. Several alternatives were possible but neither of them was found totally satisfactory. SEM scanning is prone to beam shifts [41], limiting the strain resolution to no more than 5×10^{-3} and requires a small test machine to go into the vacuum chamber. Digitizing times are also rather long. Optical microscopy is cheap and flexible but the very small depth of focus is a real problem because some amount of out-of-plane deformation is difficult to avoid during the test. The other point is that an intensity contrast has to be present, which is more difficult to provide with photolithography. As for using an AFM, only very small fields of view can be obtained and, again, the digitizing times are rather long. An alternative that does not seem to have been used yet is to take advantage of a white light interferometer, which is usually used for surface roughness measurements. It will read the grid as a surface profile and will be insensitive to out-of-plane displacements. The only drawback is that there will be a limitation in terms of grid pitch, with a minimum of about 2 μm but this is compatible with the above requirements.

The next section presents the first step: the fabrication of the grids by direct interferometric photolithography.

3. Making the grids

In order to manufacture a periodic grating with a micron pitch on a surface, two major options can be distinguished.

On the one hand, sequential methods using the scanning of a beam to "draw" lines with a periodic pitch at the surface to be studied can be used. The beam can be an electron beam [4,5,7,41–43] or a FIB [8,6]. The lines can be directly milled on the studied surface (metallic for instance) if the beam is powerful enough (especially with a FIB) or on an additional layer of polymeric material. This kind of lithography allows to produce grids with pitches from a few tens of nanometers up to a few tens of micrometers but it is time consuming and therefore not well suited for large scale patterning. Another important limitation lies in the size of the processed sample which is limited by the size of the vacuum chamber.

On the other hand, the grating can be obtained by photolithography using a photoresist deposited on the sample. This is usually done through a mask [3,6,44,45]. The advantage of this technique is to produce gratings very quickly. Usual pitches are from 1 μm up to a few tens of micrometers.

In the proposed approach, no physical mask is used. The grating is directly produced by the interference fringes of two coherent laser beams on the photoresist (Fig. 1). Therefore, it will be called: *direct interferometric photolithography*. This type of photolithography has numerous advantages compared to the mask lithography: the grid pitch and size can be easily adjusted and the problems faced with mask alignment are avoided. Another aspect is that, as it was shown on porous silicon, if the material under study is "photosensitive", it allows a direct patterning without the need of any photoresist [46].

In practice, the laser beam is first expanded and filtered through a set of lenses and a pin-hole to get the required diameter. It is then split-up in two beams of equal intensity that are reflected by two mirrors onto the sample previously coated with the photoresist. The pitch p of the grid thus obtained is simply given by the interferometry law:

$$p = \frac{\lambda}{2 \sin \theta}, \tag{3.1}$$

where λ is the wavelength of the laser beam and θ, the angle of incidence.

In order to obtain a 2D grid, the solution is to illuminate first in one direction and then to rotate the sample by 90° and illuminate a second time.

Although this patterning technique is not new, its application to mechanics is quite original. Compared to moiré interferometry that uses the same kind of gratings, the grid making does not here imply a step of replication from a master grid (assumed to be perfect) [18] as they are directly marked onto the sample. This option is much more convenient and easier as the replication process is difficult to develop and can potentially reduce the quality of the grids. To the best knowledge of the present authors, this

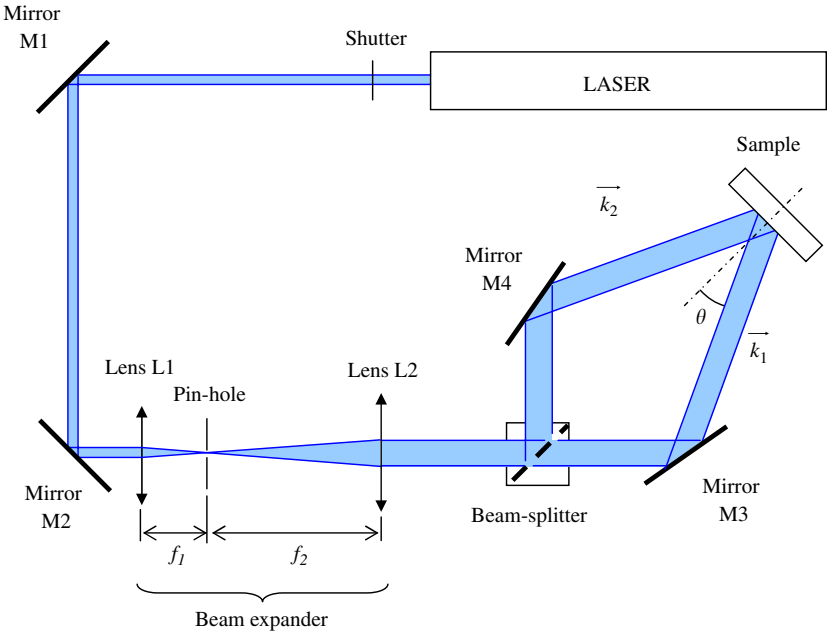

Fig. 1. Interferometric setup.

direct marking of the sample has only been applied till now to "electronic" substrates (such as Si or AsGa substrates) that are perfectly plane and without polishing scars or surface defects. Its application to an engineering material such as steel is new.

The light source is a 150 mW, 441.6 nm wavelength single mode (TEM_{00}) Helium–Cadmium laser (Kimmon Electric Co. Ltd.). The interference fringes are exposed on a positive photoresist (commercially referenced as Shipley Microposit® S1813) spin coated on the sample, previously polished down to a 1 μm finish, so as to get a layer with a constant thickness of 0.5−1 μm (typically 6000 rpm during 30 s). The sample is then soft baked at 120 °C on a hotplate during 1 min 30 s in order to evaporate the solvent from the photoresist.

4. Characterization of the grating shape

In order to characterize the shape of the gratings obtained with the direct interferometric photolithography, their 3D profile was examined using an AFM (M5, Park Scientific Instrument) (Fig. 2). These measurements have been made for several exposure doses, 300 mJ/cm^2, 500 mJ/cm^2 and 1 J/cm^2 (these values correspond to the intensity of the bright interference peak).

Theoretically, this shape should be sinusoidal (as the interference fringes are). But in fact, the response of the photoresist against the exposure dose is not linear but given by the so-called "contrast curve" of the resist (Fig. 3). When integrating this non-linearity, the theoretical shapes can be plotted for different exposure doses and compared to the experimental ones. Figs. 4–6 show an extracted profile from the AFM measurements for the three different exposure doses considered and the corresponding theoretical profiles. It can be observed that the profiles are globally similar. The slight differences can be explained by the fact that the illumination is not exactly homogeneous and can be locally disturbed. Additionally, the substrate itself is reflective and the incident beams can interfere with the reflected ones creating fringes in the direction normal to the surface of the sample. This will lead to a "staircase effect" that can be seen on Fig. 2. This effect, well known in photolithography, can be almost suppressed by using a so-called antireflection coating (ARC) deposited prior to the photoresist.

5. Optimization of the grids

In order to optimize the quality of the displacement measurements that will be obtained, a preliminary study has been carried out on the grids. The choice was to concentrate the efforts on the major parameter involved in making the grids, that is to say, the exposure dose. The objective function to be minimized was the displacement resolution: with the *grid method*, this parameter is directly related to the phase noise.

5.1. *The grid method [23]*

This method is a geometric optical method to measure displacement fields. The main assumption of this method is to consider that the deposited grid perfectly follows the deformations of the substrate.

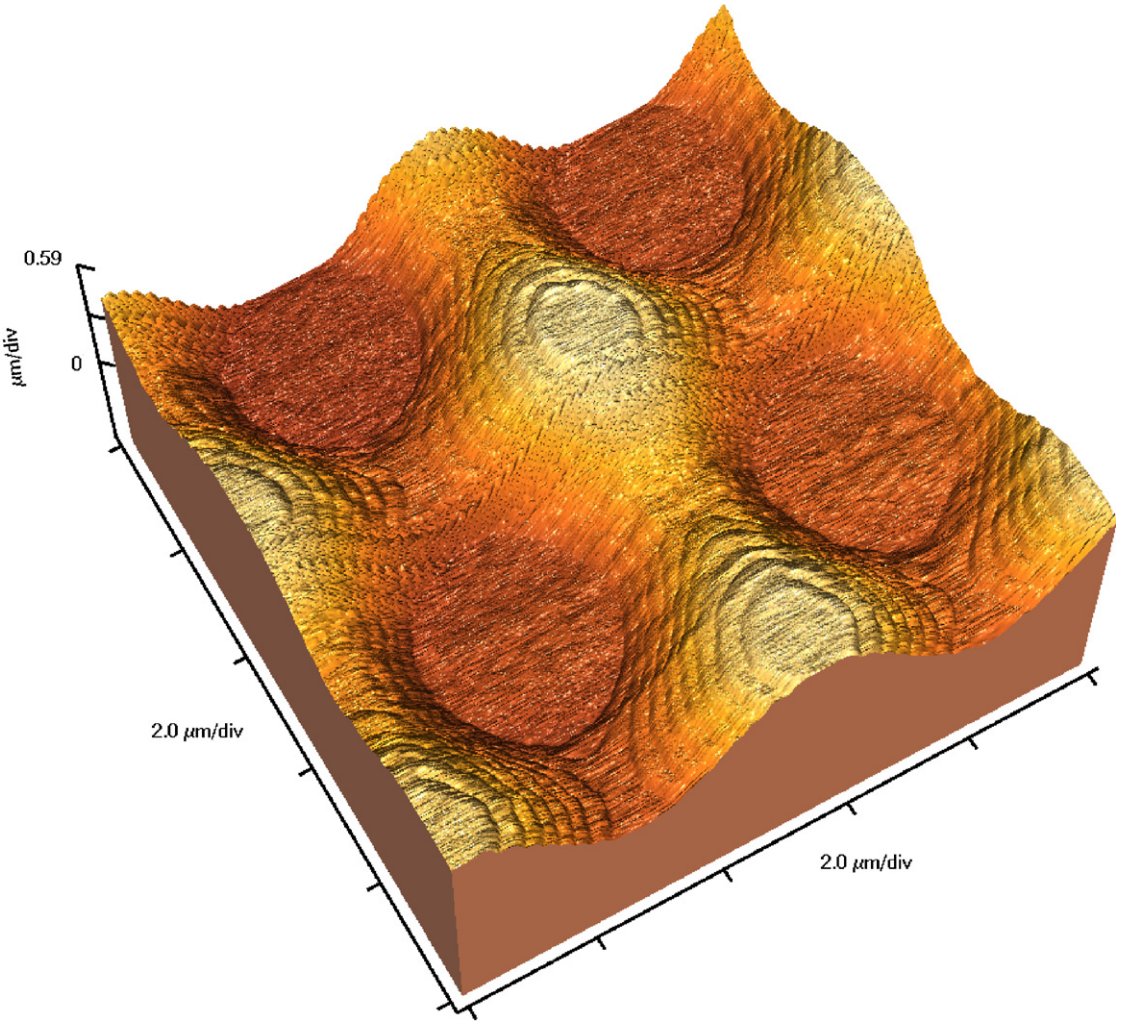

Fig. 2. 3D profile of a grating obtained with an AFM.

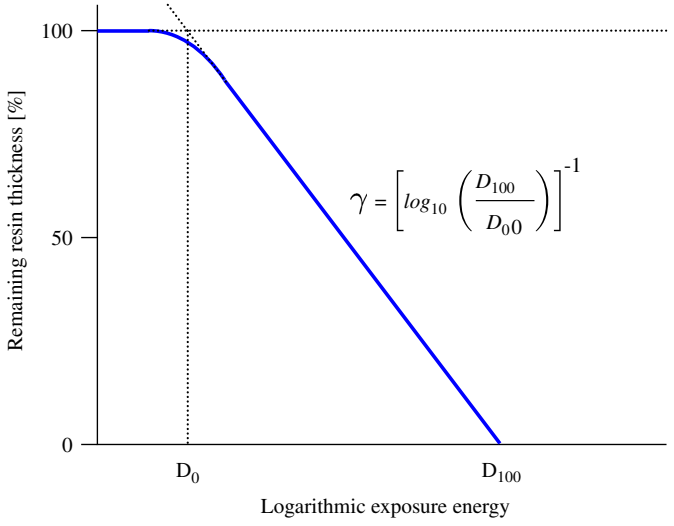

Fig. 3. Contrast curve of the photoresist.

5.1.1. *Phase modulation*

The function of the grid is to be a spatial carrier. A cross grid, which allows to get the two components of the in-plane displacement, is considered here. The intensity reflected at a point of coordinates (x, y) is

$$I(x,y) = I_0(x,y)\left[1 + \gamma(x,y)\,\mathrm{frgn}\left(\frac{2\pi x}{p}\right)\mathrm{frgn}\left(\frac{2\pi y}{p}\right)\right], \tag{5.1}$$

where:

- $I_0(x, y)$ is the mean intensity;
- $\gamma(x, y)$ is the local contrast,
- frgn() is a periodic function which frequency is $f = 1/p$.

It must be noted that when the grids are observed with an optical microscope, it is indeed the light intensity that bears the information but when the white light interferometer is be used, the signal is a vertical position $z(x, y)$.

The x and y information has to be separated before being processed. A simple way to achieve this is to perform a spatial averaging over one period in the discarded direction.

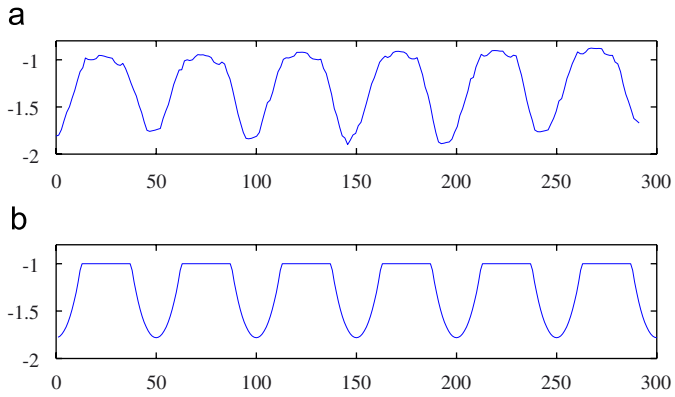

Fig. 4. Profile of the grating for an exposure dose of 300 mJ/cm^2. (a) Practical profile; (b) theoretical profile.

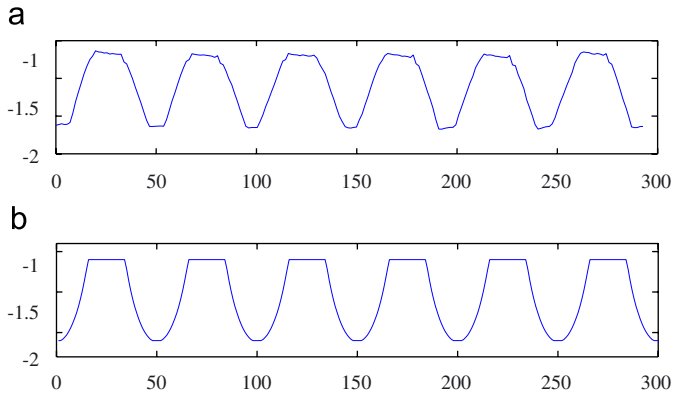

Fig. 5. Profile of the grating for an exposure dose of 500 mJ/cm^2. (a) Practical profile; (b) theoretical profile.

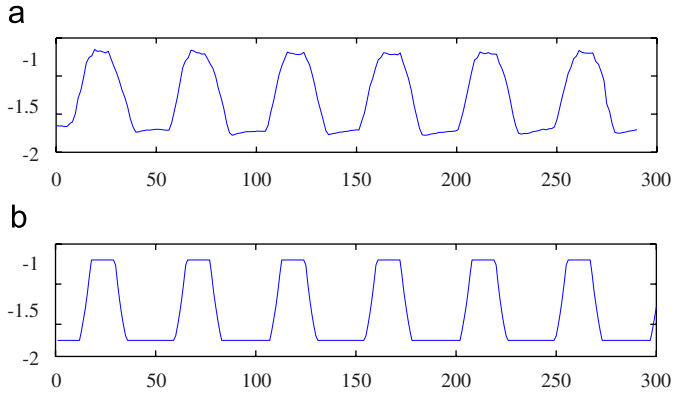

Fig. 6. Profile of the grating for an exposure dose of 1 J/cm^2. (a) Practical profile; (b) theoretical profile.

When a load is applied, the x and y displacement fields can be considered as two phases superimposed to the periodic signal. By detecting the phases at each point before and after applying the loads and by subtracting them, $\Delta\phi_x$ and $\Delta\phi_y$, directly proportional respectively to u_x and u_y, the two components of in-plane Lagrangian displacement, are obtained all over the studied surface [23]:

$$\begin{cases} u_x(x,y) = -\dfrac{p}{2\pi}\Delta\phi_x(x,y), \\ u_y(x,y) = -\dfrac{p}{2\pi}\Delta\phi_y(x,y). \end{cases} \tag{5.2}$$

5.1.2. Spatial phase-shifting algorithm

It has been shown in the previous section that the important parameter to be considered is the phase. An appropriated algorithm has to be defined to extract it from the intensity signal.

In Eq. (5.1), there is an infinity of unknown parameters: A, γ, the phase and the Fourier coefficients of the frgn function. Considering that the frgn function is harmonic, the number of unknown parameters goes down to 3: A, γ and the phase. It is therefore necessary to get at least three equations to be able to solve the problem and extract the phase from the signal. Two main approaches are available:

- spatial phase shifting: the information is searched at the vicinity of the considered pixel;
- temporal phase shifting: the information is searched at the considered pixel but on recordings taken at different moments.

The first technique is chosen here because temporal phase shifting is difficult to perform at this scale and also because it leads to much longer acquisition times. The principle is to get several samples I_k, $k = 0, 1, \ldots, M-1$ separated by a constant phase shift δ:

$$I_k = I(\phi + k\delta). \tag{5.3}$$

These sampling points enable the determination of the best fitting harmonic function. With this approach, the general form of the phase detection algorithm is

$$\phi = \arctan\left[\frac{\sum_{k=0}^{M-1} b_k I_k}{\sum_{k=0}^{M-1} a_k I_k}\right]. \tag{5.4}$$

The quality of the phase strongly depends on the way the a_k and b_k coefficients are chosen.

By choosing a windowed-DFT algorithm (DFT stands for "discrete-Fourier-transform") with a triangular windowing, harmonics are eliminated up to the $(N-2)$ order (N is the number of pixels sampling one period of the signal) and the influence of the uncertainty on the calibration (number of pixels per period i.e., N) is reduced [47]. The latter can be written as follows:

$$\phi = \arctan\left[-\frac{\sum_{k=1}^{N-1} k(I_{k-1} - I_{2N-k-1})\sin(2k\pi/N)}{NI_{N-1} + \sum_{k=1}^{N-1} k(I_{k-1} - I_{2N-k-1})\cos(2k\pi/N)}\right]. \tag{5.5}$$

Considering its numerous advantages, the windowed-DFT algorithm has been chosen here.

5.2. Optimization of the exposure dose for an observation with an optical microscope

As said before, it has been chosen to optimize the exposure dose in order to minimize the average phase noise obtained with the *grid method* for an image of a given grid. In practice, two images of the same grid are recorded (without loading the sample between the two recordings) and their phase map is calculated. At a given point, the phases obtained can be given by the following equation:

$$\begin{cases} \phi_1 = \phi + n_{\phi_1}, \\ \phi_2 = \phi + n_{\phi_2}, \end{cases} \tag{5.6}$$

where ϕ_1 and ϕ_2 are the recorded phases, ϕ is the actual phase and n_{ϕ_1} and n_{ϕ_2} are the recorded noises (assumed here to be Gaussian). By subtracting the two phase maps, only the difference of the noises remains:

$$\phi_2 - \phi_1 = n_{\phi_2} - n_{\phi_1}. \tag{5.7}$$

The variance of each phase noise is σ_ϕ^2. The variance of the subtraction $n_{\phi_2} - n_{\phi_1}$ will be $2\sigma_\phi^2$. The displacement resolution can be quantified by the standard deviation of the displacement which is equal to $(p/2\pi)\sqrt{2\sigma_\phi^2}$.

The exposure dose has been studied in the (100–1600) mJ/cm^2 range with an increment of 100 mJ/cm^2

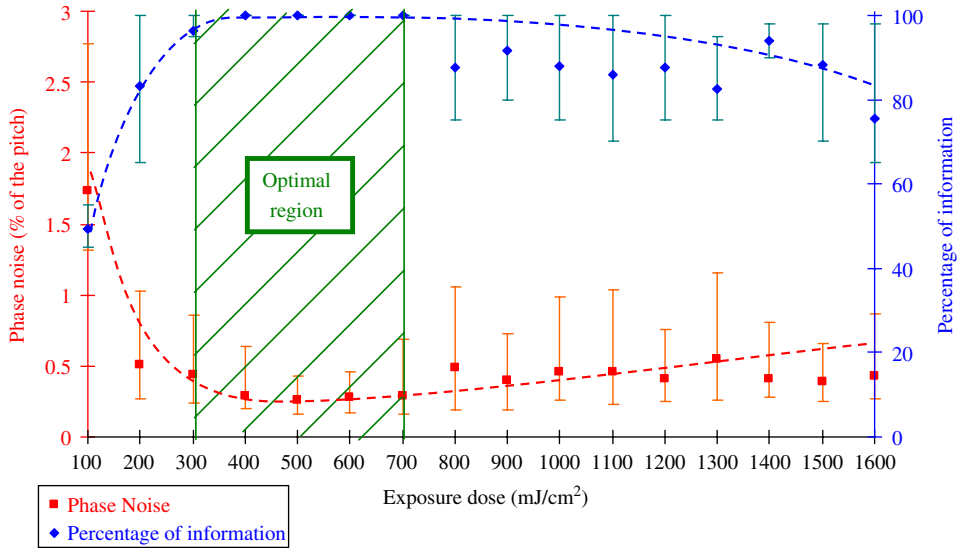

Fig. 7. Phase resolution and percentage of relevant information obtained with an optical microscope plotted against exposure dose.

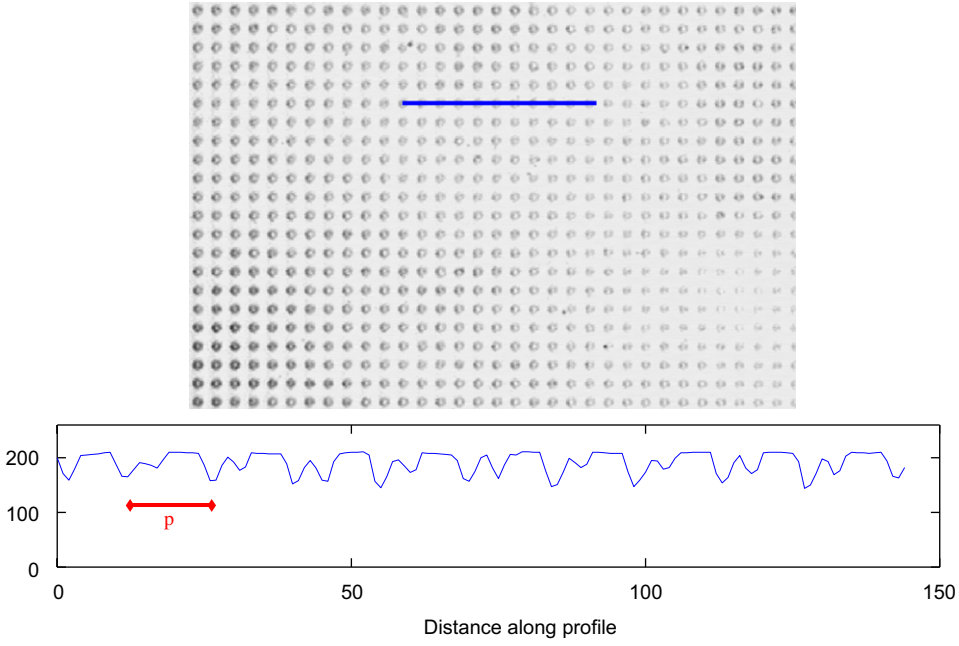

Fig. 8. Profile of the optical image of the grating for an exposure dose of 200 mJ/cm^2.

(considering the maximum intensity of the bright fringe). Tests have been made on 6 batches of 16 samples marked with cross grids of 5.6 μm pitch. Five different observations have been carried out for each grid. Observations have been made using an optical microscope with a 50× objective and a CCD camera of 574 × 760 pixels with a sampling of 15 pixels per period. The average results are shown in Fig. 7.

Moreover, it has to be mentioned that during phase shifting, regions of the image that do not present enough contrast are not processed. No phase value is obtained for the corresponding pixels. These pixels represent a loss of relevant information. For each value of exposure dose, this loss can be approximately determined. Fig. 7 also shows the percentage of relevant information as a function of the exposure dose. The percentage of relevant information is defined as the ratio between the number of pixels for which a phase value is obtained over the total number of pixels.

By observing these two curves, a range of optimal intensity can be determined: by choosing the exposure dose between 400 and 700 mJ/cm^2, the displacement resolution appears optimized and the percentage of relevant information is 100%.

The most probable explanation of this optimal range is the following:

- under 400 mJ/cm^2, the luminous contrast is not enough to get a high-quality information: consequently, the

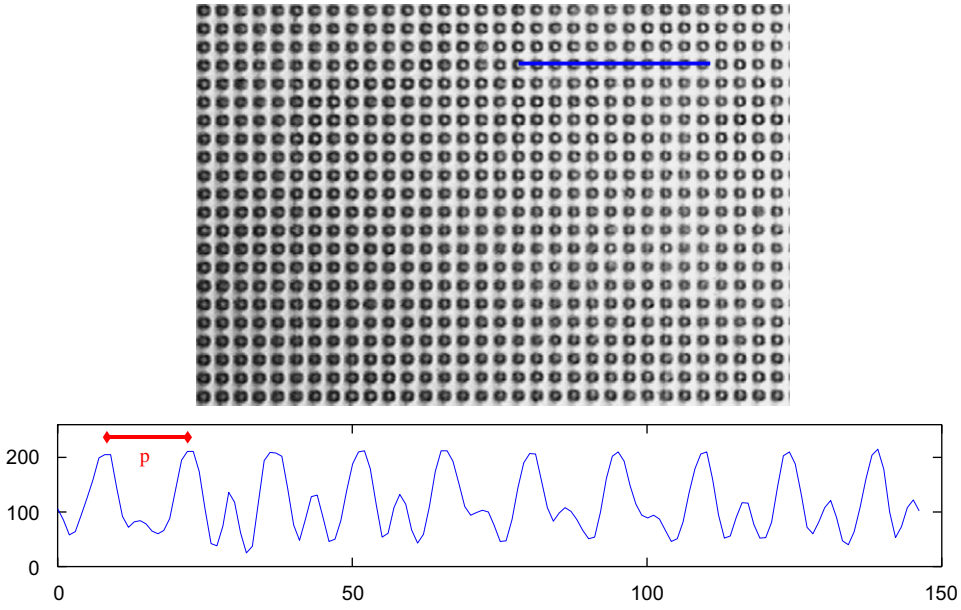

Fig. 9. Profile of the optical image of the grating for an exposure dose of 500 mJ/cm^2.

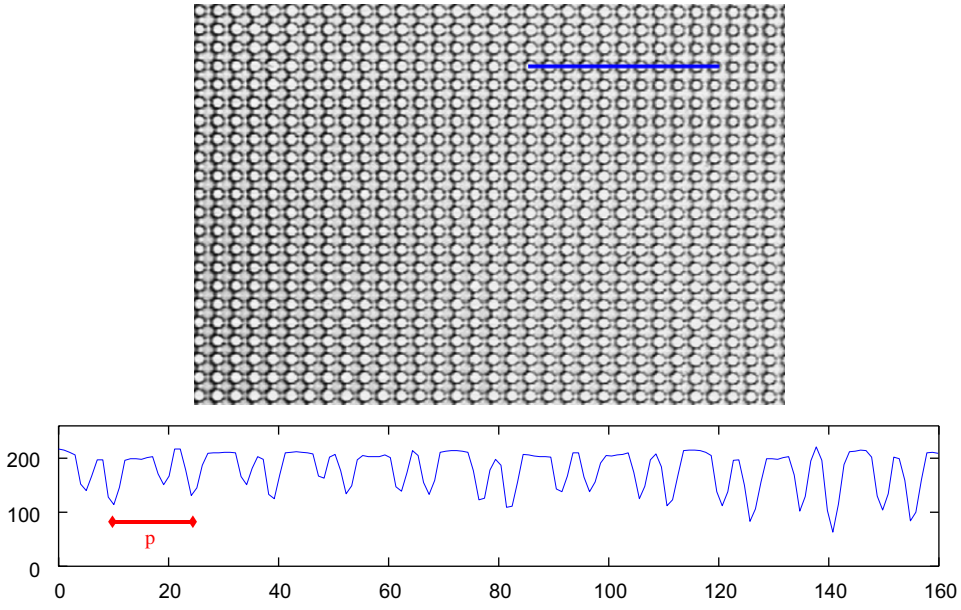

Fig. 10. Profile of the optical image of the grating for an exposure dose of 1 J/cm^2.

relative part of the noise is very high and the percentage of relevant information is quite low;

- beyond 700 mJ/cm^2, under the optical microscope, the two flat surfaces are reflecting the light whereas the slopes are not (Fig. 6). The white/black pattern appears twice within the pitch width. Consequently, there is a strong influence on the first harmonic hence a high level of noise Figs. 8–10.

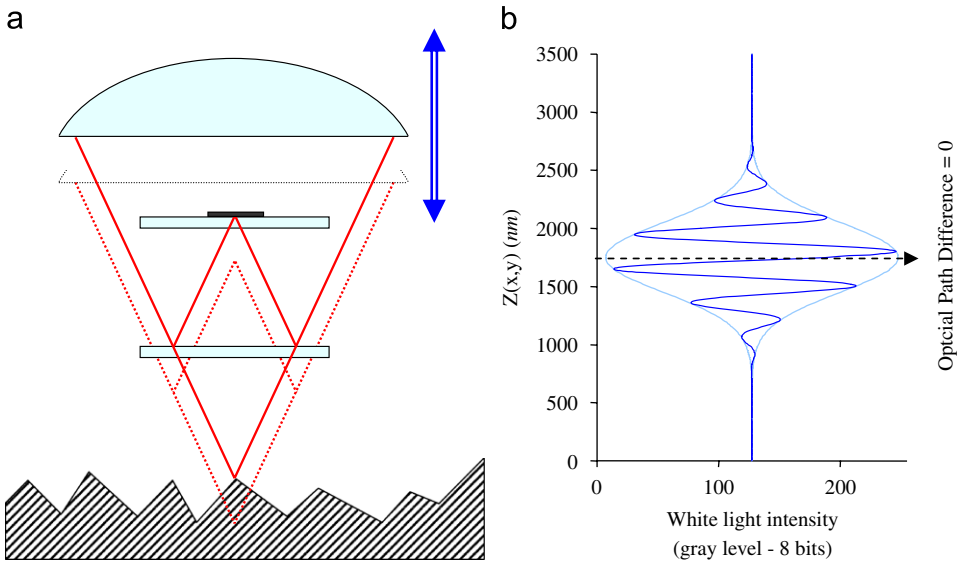

Fig. 11. Principle of a white light interferometer: (a) interferometric lens (“Mirau” type); (b) white light interference fringes.

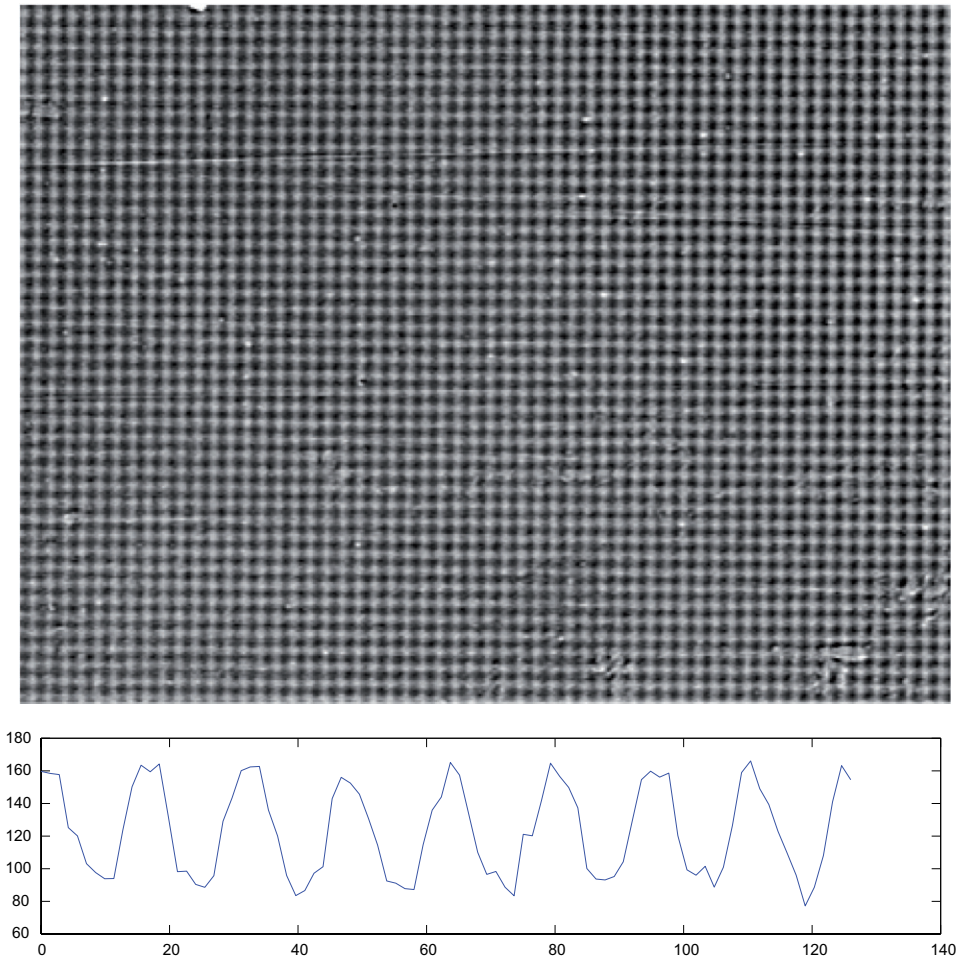

Fig. 12. Profile of an image of the grating obtained with a white light interferometric microscope for an exposure dose of 100 mJ/cm^2.

In any case, the raw signal is rather far from a harmonic one and this digitization technique has been abandoned. The idea is to measure the surface profile using a white light interferometer. This is the object of the next section.

5.3. *Optimization of the exposure dose for an observation with a white light interferometer*

5.3.1. *Principle of a white light interferometer [48]*

White light interferometry is a non-contact, optical technique for measuring surface topography.

White light, coming from an interferometric lens, passes through a beam splitter, which directs the light to the sample surface and a reference mirror (Fig. 11(a)). When the light reflected from these two surfaces recombines, a pattern of interference "fringes" forms. For each point of the sample, maximum fringe contrast occurs when the optical path difference (OPD) is equal to 0 (this effect is much more obvious with white light because of its short coherence-length). The reference inside the lens is adjusted such as this maximum corresponds to the best focus position (Fig. 11(b)): determining the z position of this maximum amounts to determining the z position of the considered point of the surface under study. For that, the interferometric lens scans vertically the surface to study while the CCD sensor records the intensity history for each pixel. Then, the system determines the maximum of amplitude of the fringes (by taking the maximum of the envelope curve for instance) and thus determines the altitude of every point of the observed surface.

This method is short (a few seconds) and very sensitive (subnanometric resolution in the z direction).

5.3.2. *Observation of the grids with a white light interferometer*

The same kind of optimization has been performed for an observation with a white light interferometer as for an observation with an optical microscope.

With this device, the observation requires more care than with a classical optical microscope:

- due to the characteristics of the interferometric lenses, the profiler cannot obtain a measurement on a surface with a local slope of more than approximately 30° (whereas, for a non-interferometric lens, slopes up to 50° can be observed);
- semi-transparent materials are very difficult to characterize.

These two restrictions impose in practice to have rather shallow grid patterns (with a lower exposure dose) and to

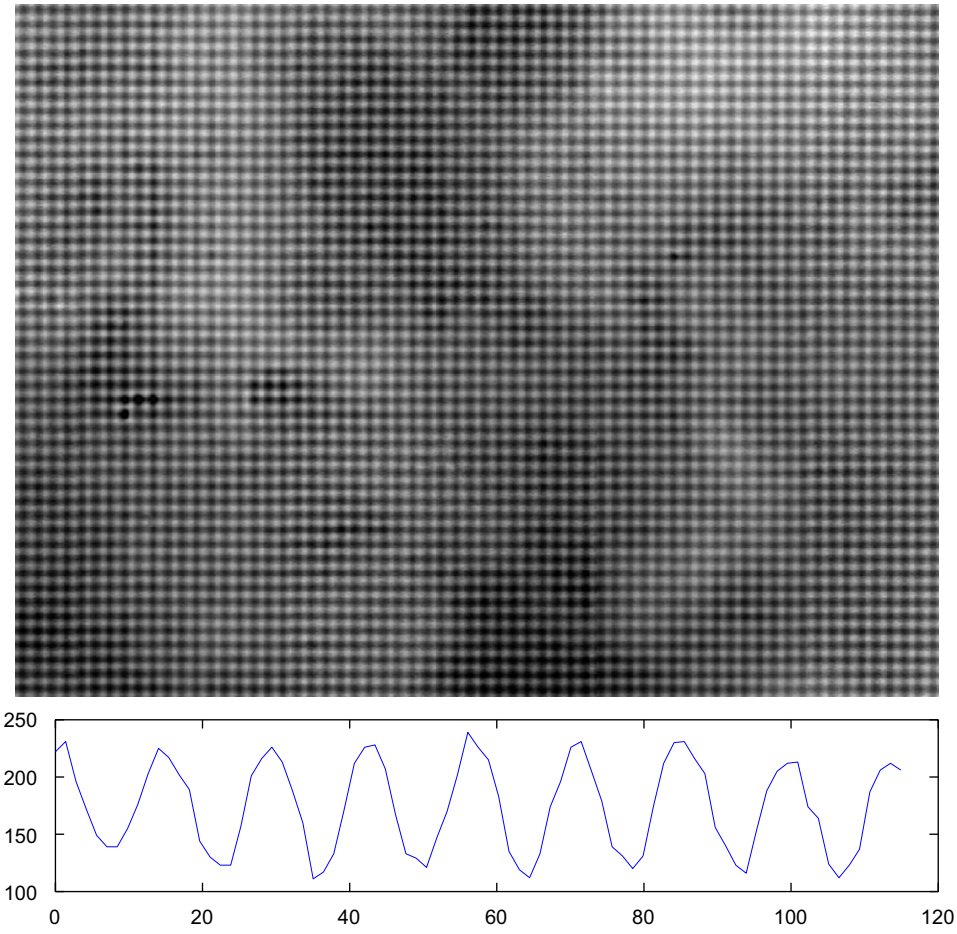

Fig. 13. Profile of an image of the grating obtained with a white light interferometric microscope for an exposure dose of 150 mJ/cm^2.

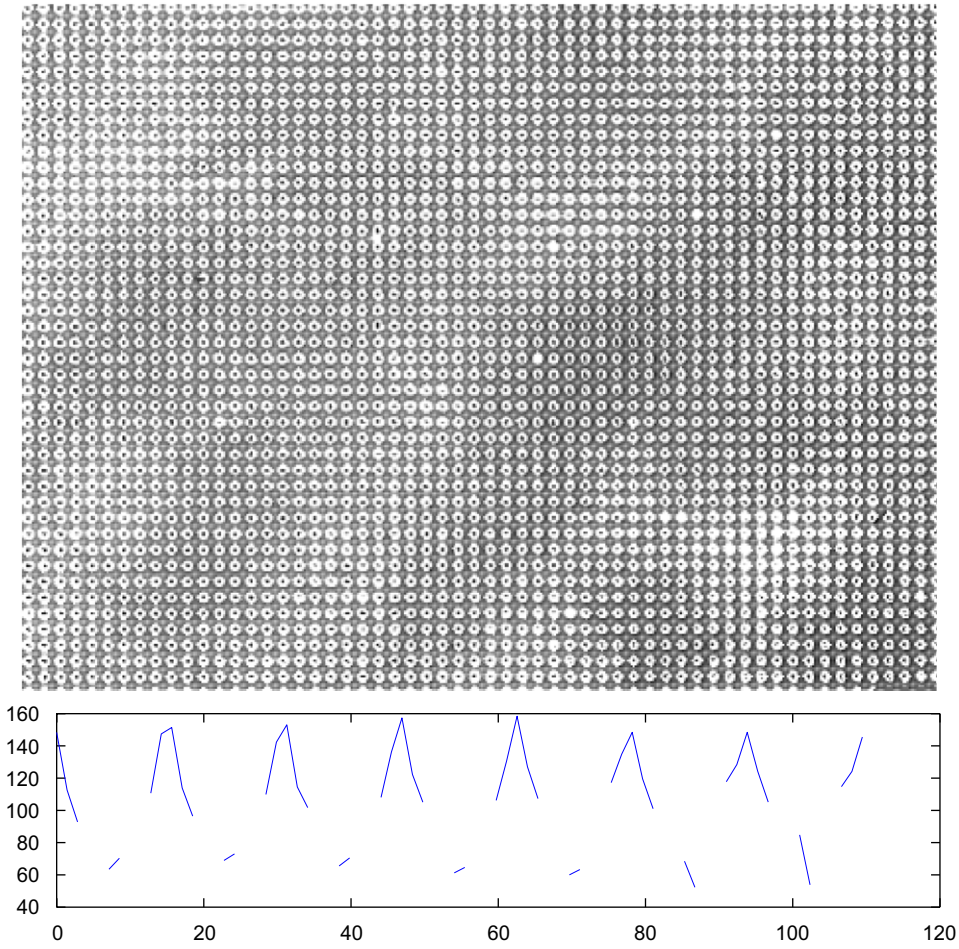

Fig. 14. Profile of an image of the grating obtained with a white light interferometric microscope for an exposure dose of 400 mJ/cm^2.

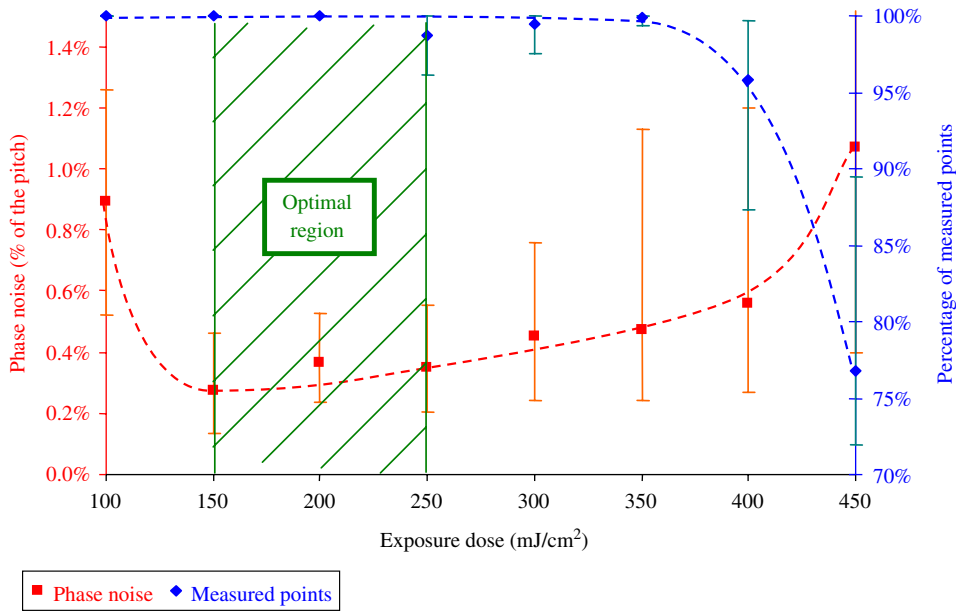

Fig. 15. Phase resolution and percentage of measured points obtained with a white light interferometer plotted against exposure dose.

coat them with a thin layer of metal to get a reflective surface. Platinum deposited by ion sputtering was used here as a reflective coating.

The exposure dose has been studied in the range $(100-450)\,mJ/cm^2$ with an increment of $50\,mJ/cm^2$ (considering the maximum intensity of the bright fringe). Tests have been made on 2 batches of 8 samples marked with cross grids of 5.6 μm pitch. Five different observations have been carried out for each grid produced using a white light interferometer (Veeco®, Wyko NT3300) with a 20× lens and recorded thanks to a CCD camera of 480 × 640 pixels with a sampling of 11 pixels per period (Figs. 12–14). Fig. 15 shows the average noise and the percentage of measured points (points where local slopes can be measured by the white light interferometer) as a function of the exposure dose.

The optimal range of exposure dose for the white light interferometer can be chosen between 150 and $250\,mJ/cm^2$: the displacement resolution is minimized and the percentage of measured points is approximately 100%.

6. Study of the numerical rigid body motion

Keeping in mind the final application of the grids, i.e., the measurement of the in-plane displacement field at the surface under study, a rigid body motion has been applied to the grid to evaluate the displacement resolution. As a first step and because it is more convenient (experimental rigid body motion with a relevant precision is difficult to obtain at this scale), it was decided to numerically investigate this effect on experimental grid images. This consisted in the following:

- the "initial state" is a real experimental image from the white light interferometer;
- the "final state" is the same image but shifted of a whole number of pixels in the x direction.

The images were taken using a 50× lens with a 0.5× zoom, leading to a sampling of 14 pixels per period.

This procedure has been applied with a pitch of one pixel over a range covering four periods of the grid. The standard deviation of u_x and u_y can be plotted against the numerical displacement (Fig. 16). It can be seen that this value monotonically increases with the numerical displacement. This was observed even for u_y which should not be substantially affected since the imposed displacement is in the x direction.

These results are not enough to draw a clear conclusion. The phenomenon taking place has to be investigated more precisely.

By looking at the u_x (Fig. 17) and u_y (Fig. 18) displacement maps, it can be seen that the noise is spatially correlated. In order to improve the accuracy and the resolution of the displacement measurement, it is necessary to determine the origin of this correlation. Several origins can be expected for the presented results.

The variations of contrast of the grid have been thought to be responsible of the correlation of the noise. Indeed, the lower the contrast, the more the noise influences the results (as its relative part increases). This hypothesis has been rapidly turned down. A simulated noisy grid with a comparable contrast has been generated and processed with a numerical rigid-body motion as explained above. The standard deviation of the displacement values is getting constant after a displacement equal to one pitch and with a lower level (around 0.9% of the grid pitch). Moreover, the displacement maps exhibit a fully spatially independent noise. For example, Fig. 19 shows the results obtained for such simulated grids. Grids were coded on 255 gray levels with a white noise presenting a standard deviation of 20 gray levels i.e., a signal to noise ratio equal to 40 which is rather poor.

The observed deterioration of the displacement maps can be due to the grid itself. It can be due to the presence of

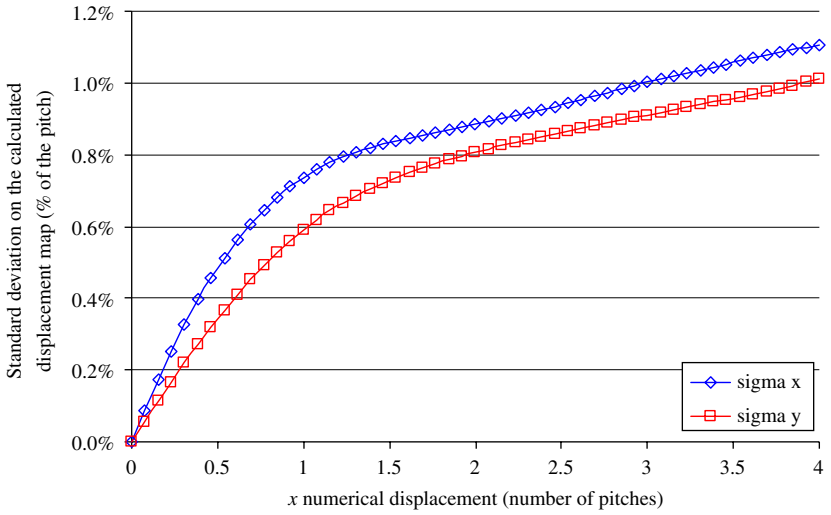

Fig. 16. Standard deviation of the calculated maps of u_x and u_y plotted against the numerical displacement.

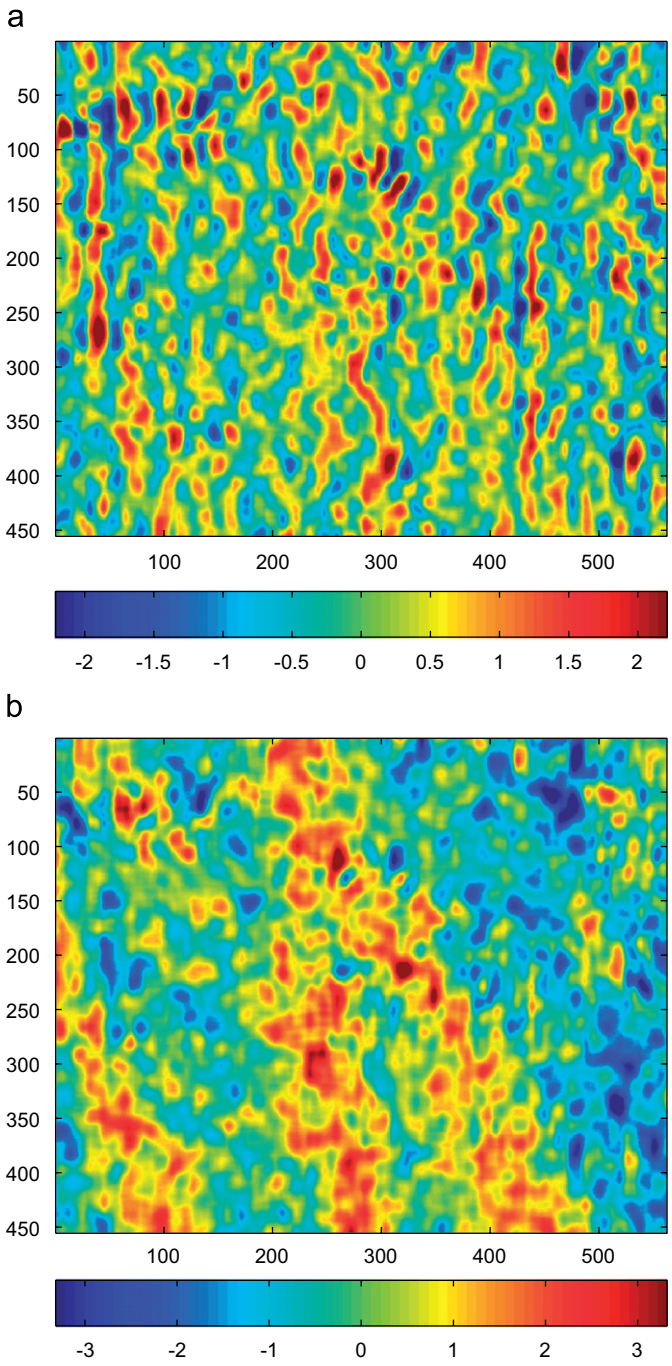

Fig. 17. ($u_x - u_{x_{\text{average}}}$) maps for two different numerical imposed x displacements (colormap values in percentage of the pitch).

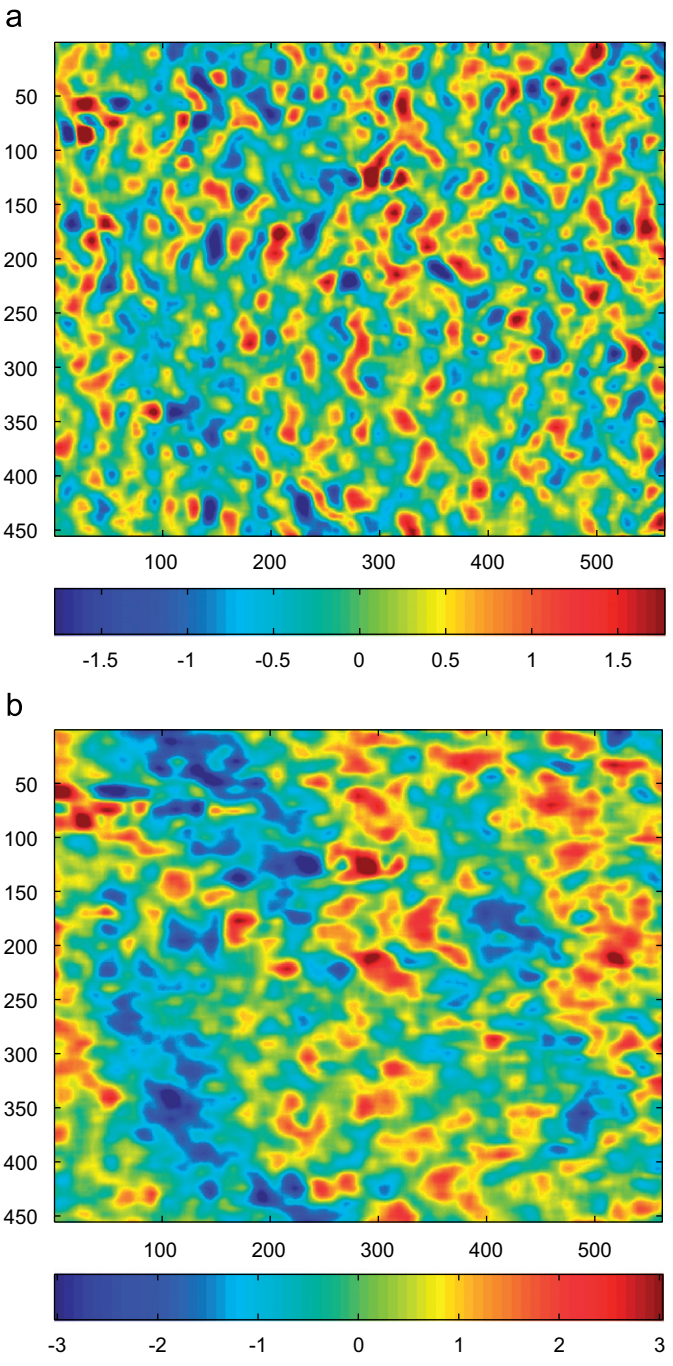

Fig. 18. ($u_y - u_{y_{\text{average}}}$) maps for two different numerical imposed x displacements (colormap values in percentage of the pitch).

polishing scars or inclusions locally disturbing the detection of the phase or the presence of harmonics in the grid signal, ...or to the observation instrument. Further investigations are actually needed to determine precisely the origin of the phenomenon. Nevertheless, the performances of the technique are already rather good, with a displacement resolution of about 1% of the grid (here, 56 nm), with a spatial resolution of 5.6 μm. Pitches down to about 2 μm can be used. The final strain resolution will depend on the smoothing procedure used. This is the next step.

7. Conclusion

In this study, the manufacturing of micrometric gratings by direct interferometric photolithography has been proposed and demonstrated. An optimization of the relevant parameters has been obtained taking into account the specific mechanical application they are designed to. This optimization consisted in finding the exposure dose that minimized the phase-noise of the image of the grating obtained with an optical microscope or with a white light

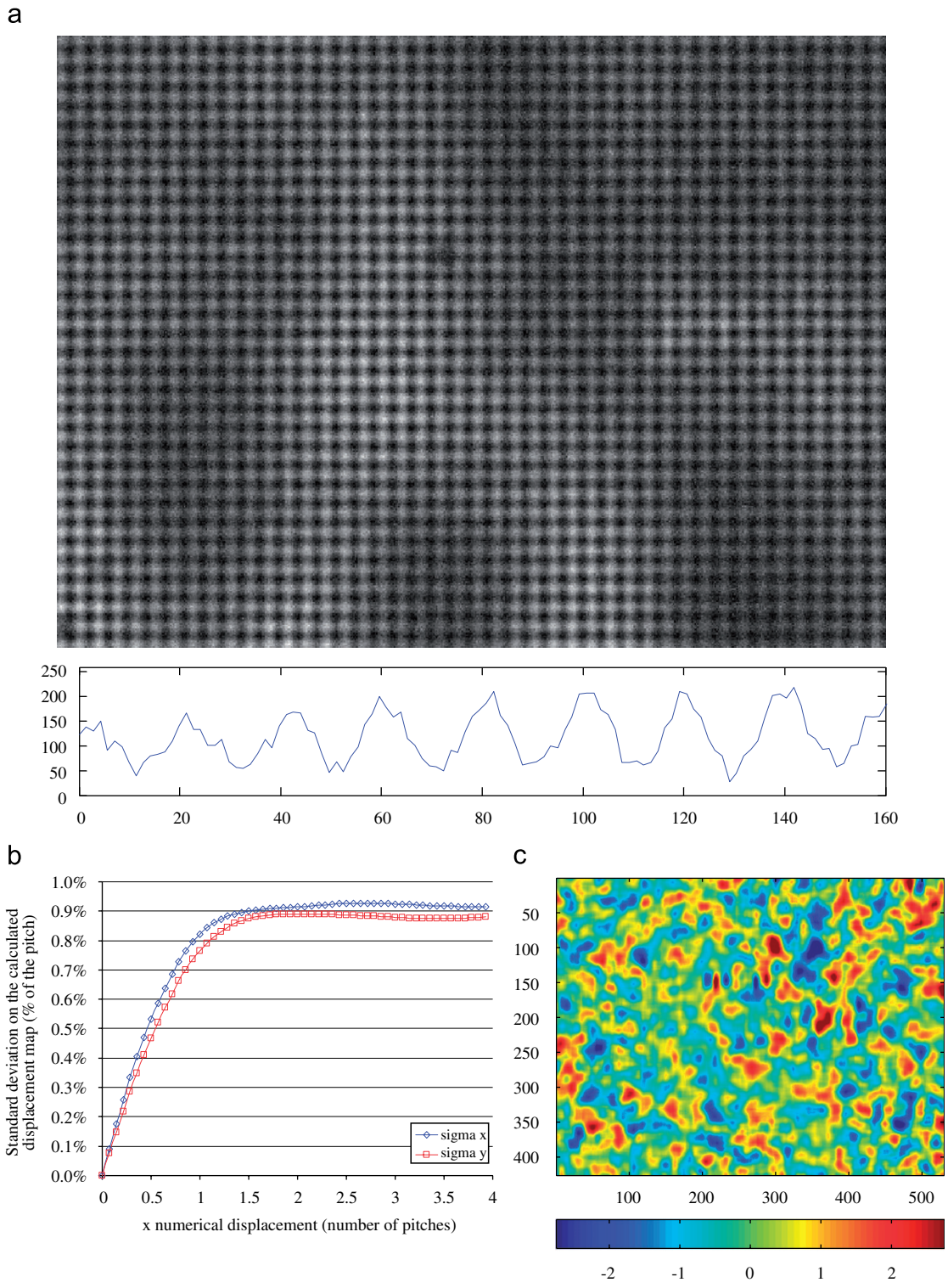

Fig. 19. Results obtained for a simulated grid with variable contrast and white noise: (a) simulated grid; (b) standard deviation plotted against the numerical displacement; (c) $(u_x - u_{x_{\text{average}}})$ map for an imposed x displacement $= 4 \times p$ (colormap values in percentage of the pitch).

interferometer and processed with the specific spatial phase-shifting algorithm of the grid method. A numerical rigid body motion from experimental images has been finally addressed and has underlined some spatial correlation problems that will possibly occur during a real mechanical test. To reduce these effects, several palliative options are envisaged and will be attempted in the near future:

- optimize the kinematic chain of the future testing apparatus in order to avoid or at least reduce the rigid body motion (symmetry of the loading system, etc.);

- slightly increase the thickness of the photoresist layer to try to fill in the polishing scars and all other topographic defaults occurring over the surface but without modifying the mechanical properties of the substrate;
- investigations are currently being carried out to determine if the main cause of the problem is due to the grids themselves or to the white light interferometer. The results will induce corrective actions (improvement of the device or of the quality of the grids, use of numerical procedures to limit the influence of defaults, ...).

Finally, it must be noted that the present approach is original and represents a promising alternative to existing techniques, even if it is still under development. One possible perspective lies in the measurement of local strain fields at the surface of metallic alloys under tensile load in order to identify the local elasto-plastic constitutive equations and more especially, the local elastic limit, in order to correlate results obtained by heat dissipation measurements [49].

Acknowledgments

This research has been conducted within the framework of the ''NANODEF'' project financially supported by the French Ministry for Research and the Champagne-Ardenne Regional Council.

References

[1] Amidror I. The theory of the moiré phenomenon. Dordrecht: Kluwer Academic Publishers; 1999.
[2] Asundi A. Computer aided moiré methods. Opt Lasers Eng 1993;18:213–38.
[3] Read DT, Dally JW, Szanto M. Scanning moiré at high magnification using optical methods. Exp Mech 1993;33:110–6.
[4] Chen H, Liu D. Advances in scanning electron microscope moiré. Exp Mech 2001;41:165–73.
[5] Dally JW, Read DT. Electron beam moiré. Exp Mech 1993;33:270–7.
[6] Xie H, Liu Z, Fang D, Dai F, Gao H, Zhao Y. A study on the digital nano-moiré method and its phase shifting technique. Meas Sci Technol 2004;15:1716–21.
[7] Kishimoto S, Xie H, Shinya N. Electron moiré method and its application to micro-deformation measurement. Opt Laser Eng 2000;34:1–14.
[8] Xie H, Li B, Geer R, Xu B, Castracane J. Focused ion beam moiré method. Opt Lasers Eng 2003;40:163–77.
[9] Xie H, Kishimoto S, Asundi A, Boay CG, Shinya N, Yu J, et al. In-plane deformation measurement using the atomic force microscope moiré method. Nanotechnology 2000;11:24–9.
[10] Zhong ZW, Lu YG. An AFM scanning moiré technique for the inspection of surface deformations. Int J Adv Manuf Technol 2004;23:462–6.
[11] Xie H, Asundi A, Boay CG, Yunguang L, Yu J, Zhaowei Z, et al. High resolution AFM scanning moiré method and its application to the micro-deformation in the BGA electronic package. Microelectron reliab 2002;42:1219–27.
[12] Takeda M, Ina H, Kobayashi S. Fourier-transform method of fringe-pattern analysis for computer-based topography and interferometry. J Opt Soc Am 1982;72:156–60.
[13] Morimoto Y, Fujisaa M. Fringe pattern analysis by a phase-shifting method using fourier transform. Opt Eng 1994;33:3709–14.
[14] Zhao B, Asundi A. Microscopic grid method—resolution and sensitivity. Opt Laser Eng 2001;36:437–50.
[15] Surrel Y. Fringe analysis. In: Rastogi PK, editor, Photomechanics; 2000.
[16] Xie H, Shang H, Dai F, Li B, Xing Y. Phase shifting SEM moiré method. Opt Laser Technol 2004;36:291–7.
[17] Xie H, Liu Z, Fang D, Dai F, Shang H. Development nano-Moiré method with high-resolution microscopy at FML. Opt Lasers Eng 2005;43:904–18.
[18] Post D, Han B, Ifju P. High sensitivity Moiré: experimental analysis for mechanical and materials. Berlin: Springer; 1994.
[19] Cordero RR, Lira I. Uncertainty analysis of displacements measured by phase-shifting moiré interferometry. Opt Commun 2004;237: 25–36.
[20] Labbe F, Cordero RR. Monitoring the plastic deformation progression of a specimen undergoing tensile deformation by moiré interferometry. Meas Sci Technol 2005;16:1469–76.
[21] Qing X, Qin Y, Dai F. Experimental investigation of micromechanical behavior of advanced materials by moiré interferometry. Opt Lasers Eng 1996;25:179–89.
[22] Nicoletto G. On the visualization of heterogeneous plastic strains by moiré interferometry. Opt Lasers Eng 2002;37:433–42.
[23] Surrel Y. Moiré and grid methods: a signal-processing approach. In: Pryputniewicz RJ, Stupnicki J, editors, Interferometry '94: photomechanics, SPIE, vol. 2342; 1994.
[24] Leendertz JA. Interferometric displacement measurement on scattering surfaces utilizing speckle effect. J Phys E Sci Instrum 1970; 3:214–8.
[25] Meinlschmidt P, Hinsch KD, Sirohi RS. Selected papers on electronic speckle pattern interferometry: principles and practice; 1996 [ISBN: 0-8194-2376-9].
[26] Li X, Wei C, Yang Y. Full-field and microregion deformation measurement of thin films usind electronic speckle pattern interferometry and array microindentation marker method. Opt Laser Eng 2005;43:869–84.
[27] Miao H, Gu P, Liu ZT, Wu XP, Zhao JH. Bulge deformation measurement and elastic modulus analysis of nanoporous alumina membrane using time sequence speckle interferometry. Opt Laser Eng 2005;43:885–94.
[28] Sutton MA, Wolters WJ, Peters WH, Ranson WF, McNeill SR. Determination of displacements using an improved digital correlation method. Image Vision Comput 1983;1:133–9.
[29] Chu TC, Ranson WF, Sutton MA, Peters WH. Application of digital image correlation techniques to experimental mechanics. Exp Mech 1985;25:232–44.
[30] Sun Z, Lyons JS, McNeill SR. Measuring microscopic deformations with digital image correlation. Opt Laser Eng 1997;27:409–28.
[31] Amodio D, Broggiato GB, Campana F, Newaz GM. Digital speckle correlation for strain measurement by image analysis. Exp Mech 2003;43:396–402.
[32] Vendroux G, Knauss WG. Submicron deformation field measurement: part 1. Developping a digital scanning tunneling microscope. Exp Mech 1998;38:18–23.
[33] Vendroux G, Schmidt N, Knauss WG. Submicron deformation field measurement: part 3. Demonstration of deformation determinations. Experimental Mechanics 1998;38:154–60.
[34] Cho SW, Chasiotis I. Elastic properties and representative volume element of polycrystalline silicon for MEMS. Exp Mech 2007;47: 37–49.
[35] Vogel D, Gollhardt A, Michel B. Micro- and nanomaterials characterization by image correlation methods. Sensors Actuators Part A 2002;99:165–71.
[36] Knauss WG, Chasiotis I, Huang Y. Mechanical measurements at the micron and nanometer scales. Mech Mater 2003;35:217–31.
[37] Chen J, Xia G, Zhou K, Xia G, Qin Y. Two-step digital image correlation for micro-region measurement. Opt Laser Eng 2005;43:836–46.
[38] Vendroux G, Knauss WG. Submicron deformation field measurement: Part 2. Improved digital image correlation. Exp Mech 1998;38: 86–92.

[39] Verhulp E, van Rietbergen B, Huiskes R. A three-dimensional digital image correlation technique for strain measurements in microstructures. J Biomech 2004;37:1313–20.
[40] Sutton MA, McNeill SR, Jang J, Babai M. Effects of subpixel image restoration on digital correlation error estimates. Opt Eng 1988;27:870–7.
[41] Doumalin P, Bornert M. Micromechanical applications of digital image correlation techniques. In: Jacquot P, editor. Interferometry in speckle light. Berlin: Springer; 2000.
[42] Li C-S, Orlecky LJ. Fiducial grid for measuring microdeformation ahead of fatigue crack tip near aluminium bicrystal interface. Exp Mech 1993;33:286–92.
[43] Allais L, Bornert M, Bretheau T, Caldemaison D. Experimental characterization of the local strain field in a heterogeneous elastoplastic material. Acta Metall et Materialia 1994;42(N11):3865–80.
[44] Sciammarella CA, Sciammarella FM, Kim T. Strain measurements in the nanometer range in a particulate composite using computer aided moiré. Exp Mech 2003;43:341–7.
[45] Schroeter BM, McDowell DL. Measurement of deformation fields in polycrystalline OFHC copper. Int J Plasticity 2003;19:1355–76.
[46] Lérondel G, Romestain R, Vial JC, Thnissen M. Porous silicon lateral superlattices. Appl Phys Lett 1997;71:196–8.
[47] Surrel Y. Design of algorithms for phase measurements by the use of phase-stepping. Appl Opt 1996;35:51–60.
[48] Wyant JC. White light interferometry. In: John Caulfield H, editor, Holography: a tribute to Yuri Denisyuk and Emmett Leith, SPIE, vol. 4737; 2002.
[49] Maquin F, Pierron F. Refined experimental methodology for assessing the heat dissipated in cyclically loaded materials at low stress levels. C R Méc 2007;335:168–74.